Fe_m/Au_n multilayers from first principles

Małgorzata Sternik and Krzysztof Parlinski
Institute of Nuclear Physics, Polish Academy of Sciences, Radzikowskiego 152, 31-342 Kraków, Poland

Józef Korecki
Faculty of Physics and Applied Computer Science, AGH University of Science and Technology, al. Mickiewicza 30, 30-059 Kraków, Poland
and Institute of Catalysis and Surface Chemistry, Polish Academy of Sciences, Niezapominajek 8, 30-239 Kraków, Poland

(Received 30 June 2006; published 6 November 2006)

Using the first-principle approach and direct method, the phonon dispersion relations and the stability of the Fe_m/Au_n multilayers as perfectly ordered structures consisting of Fe(001) and Au(001) monolayers have been studied. The structures with Au and Fe layer thicknesses of two or more monolayers were shown to be stable. Multilayers with either Fe or Au monolayer were found to be unstable, although stable configurations were obtained by rearrangement of the atoms according to soft mode displacements.

DOI: 10.1103/PhysRevB.74.195405 PACS number(s): 68.65.Ac, 63.20.−e, 63.22.+m

I. INTRODUCTION

The artificial multilayered structures have attracted a lot of interest due to their unique physical properties. The multilayers with a small repetition period, in which individual layers consist only of a few atomic layers, can be easily modeled theoretically. The special interest in the low periodicity Fe_m/Au_n structures arises from the fact that the atomic positions in the (001) planes of the bcc Fe crystal and the fcc Au crystal differs only by about 0.6%. Thus, there is practically no influence of the additional stresses induced by small mismatch between atomic positions on the multilayers properties. So far, the experimentally produced Fe_m/Au_n multilayers[1–3] (fabricated layer by layer by molecular beam epitaxy) were modeled theoretically[3–5] as perfectly ordered structures of the tetragonal symmetry with the in-plane lattice constant a being that of the Au crystal and with the interlayer spacing varied across the multilayer unit cell. For the monolayer periodicity, it leads to the formation of $L1_0$ alloy, which does not exist in the Fe-Au phase diagram. The Fe/Au magnetic multilayers are intensively studied both experimentally and theoretically due to very interesting phenomena like oscillating exchange coupling,[6–10] spin dependent electron transport,[11–13] or large magneto-optical anisotropy.[3,14–16]

Although a technological progress in preparation of epitaxial films with the monolayer precision makes the growing of the Fe_m/Au_n structures feasible, the formation of Fe_1/Au_1 multilayer consisting of alternating Fe and Au monolayer is still problematic. A deviation from the layered structure was suggested by the x-ray diffraction data[1,2] and by the conversion electron Mössbauer spectroscopy (CEMS).[17–19] This paper is focused on a problem of stability of the selected configurations. Using the first-principle methods we have modeled several low periodicity Fe_m/Au_n structures with minimal ground-state energy and calculated the phonon dispersion relations and the phonon density of states spectra for them. For multilayers with single Fe or Au layers the imaginary vibration frequencies (soft modes), which characterize the unstable structures, were found. To obtain the stable configuration, relaxation of atomic positions, which in consequence changed the space group and the volume of the primitive cell, was required. The search of new stable configuration was carried out using the displacement pattern corresponding to the frozen soft phonon mode. The multilayers with thicker Fe layers are stable, since they possess only positive vibrational frequencies.

II. COMPUTATIONAL DETAILS

All total energy calculations were performed within the generalized gradient approximation (GGA) method using the VASP package.[20,21] The calculations were performed on the tetragonal supercells with 32 or 48 atoms. We included eleven valence electrons for Au atoms (s^1d^{10}) and eight for Fe atoms (d^7s^1) represented by plane wave expansions with energy cutoff of 350 eV. The wave functions in the core region were obtained by the full-potential projector augmented wave (PAW) method.[22] The Brillouin zone was sampled by a $4\times4\times4$ Monkhorst-Pack mesh. During the optimization the Hellmann-Feynman forces and the stress tensor were calculated. The crystal structure optimization was finished when residual forces were less than 10^{-5} eV/Å.

The phonon dispersion relations were calculated using the direct method.[23,24] The dynamical matrix of the crystal was calculated from the Hellmann-Feynman forces generated while displacing atoms from their equilibrium positions. For Fe_m/Au_n multilayers the displacement was 0.09 Å. The number of required displacement is determined by the symmetry of the crystal and by the number of nonequivalent atoms. Finally, the phonon frequencies were obtained by the diagonalization of the dynamical matrix for each wave vector.

III. RESULTS

A. Bulk fcc Au and bcc Fe

We started the calculations from the optimization of the fcc Au and the bcc Fe crystals, which are represented by the

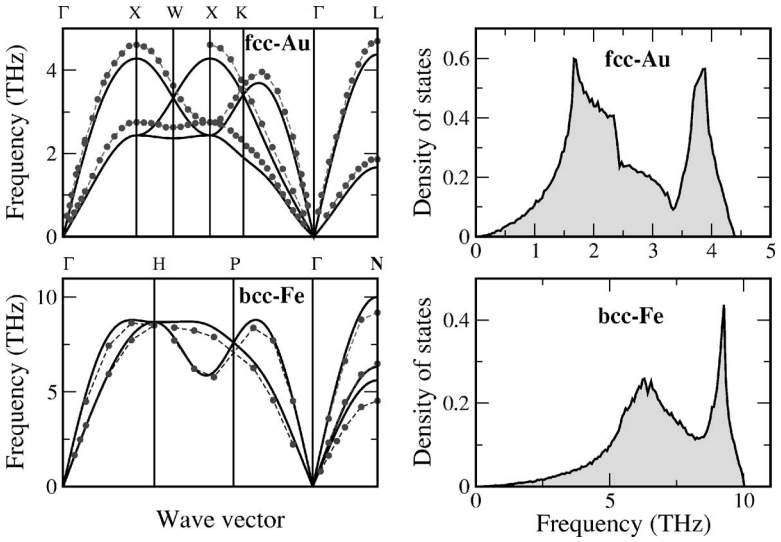

FIG. 1. The phonon dispersion relations and phonon density of states spectra for the fcc Au and bcc Fe crystals. Experimental points are taken from Refs. 28 and 29 for gold and iron, respectively.

$2\times2\times2$ supercell containing 32 Au atoms and $3\times3\times3$ supercell having 54 Fe atoms, respectively. The calculated lattice parameters of 4.14 and 2.81 Å for Au and Fe crystals, respectively, are in good agreement with experimental values of 4.08 and 2.867 Å. The obtained deviation from the experimental lattice constants (of 1.5%–2%) is typical for DFT calculations. The better agreement with experiments (0.18%) has been only reported for Fe and Ni crystals in Ref. 25. Usually, the local-density approximation (LDA) method underestimates lattice parameters, contrary, to the GGA approximation which gives overestimated values of lattice constants. In comparison to experimental lattice constants, our calculations yields too small a value for bulk Fe and too large a value for bulk Au. It results in a 2.4% mismatch between atomic positions in the (001) planes of Fe and Au crystal. Unfortunately, the calculations performed with different parameters and pseudopotentials result in the same misfit.

The spin-polarized calculations performed for the ferromagnetically ordered iron crystal do not include the spin-orbit coupling. The obtained magnetic spin moment of Fe in the bulk, 2.08 μ_B, is in accordance with measurements[26] and previous calculations.[27]

For both relaxed structures, which correspond to temperature 0 K, the phonon dispersion relations are shown in Fig. 1. The shapes of calculated and experimental curves are the same,[28,29] although the measured frequencies are shifted by about 7%. These discrepancies could be related to the difference between the experimental and calculated lattice parameters. Because of the large difference of atomic masses (the mass ratio $M_{\mathrm{Au}}/M_{\mathrm{Fe}}=3.53$), the maximum vibrational frequency of 10 THz of the lighter Fe atoms is much higher than that of 4.4 THz of the Au atoms.

B. $\mathrm{Fe}_m/\mathrm{Au}_n$ multilayers

The $\mathrm{Fe}_m/\mathrm{Au}_n$ multilayers unit cells consisting of m Fe(001) and n Au(001) monolayers are schematically presented in Fig. 2. These unit cells are repeated periodically along the z axis since the three-dimensional boundary conditions are imposed in the calculations. Each layer has a square surface unit cell with lattice constant $a=2.87$ Å. Layers consisting of four atoms placed in the corners are separated by the layers having one atom in the middle of the square. The distance between two neighboring Au layers is initially set to the value obtained for the interlayer distance in a fcc Au crystal, the distance between two neighboring Fe layers is set

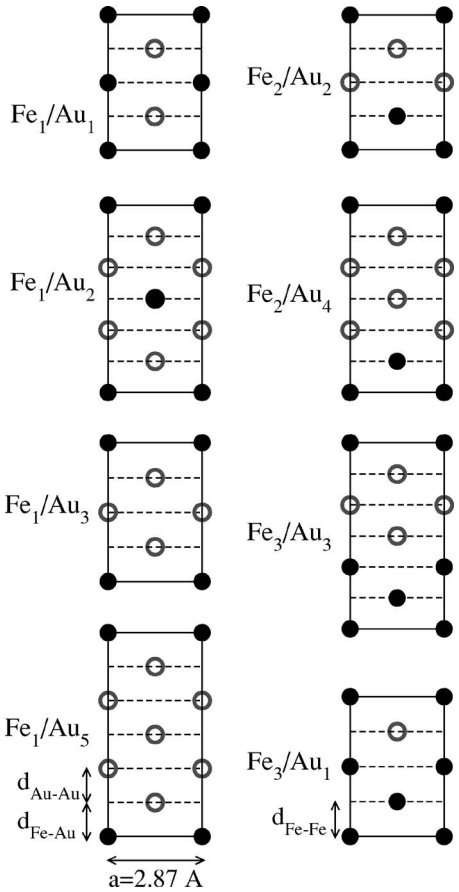

FIG. 2. The schematic pictures of the different $\mathrm{Fe}_m/\mathrm{Au}_n$ multilayers. The black and open circles represent Fe and Au atoms, respectively. The distances between different layers are $d_{\mathrm{Au\text{-}Au}}=2.07$ Å, $d_{\mathrm{Fe\text{-}Au}}=1.73$ Å, and $d_{\mathrm{Fe\text{-}Fe}}=1.40$ Å.

TABLE I. The structural properties of Fe_1/Au_n multilayers optimized within a relevant space group. The Fe-Au and Au-Au distances are vertical distances between neighboring layers. ΔE is the formation energy per one layer consisting of eight atoms.

Multilayer	Fe_1/Au_1	Fe_1/Au_2	Fe_1/Au_3	Fe_1/Au_5
Space group	D_{4h}^1	D_{4h}^{17}	D_{4h}^1	D_{4h}^1
a (Å)	2.80	2.86	2.88	2.91
c (Å)	3.86	11.86	8.07	12.16
Nonequivalent atoms	$Fe(\frac{1}{2},\frac{1}{2},\frac{1}{2})$	Fe(0,0,0)	Fe(0,0,0)	Fe(0,0,0)
	Au(0,0,0)	Au(0,0,0.345)	$Au(\frac{1}{2},\frac{1}{2},0.227)$	$Au(\frac{1}{2},\frac{1}{2},0.147)$
			$Au2(0,0,\frac{1}{2})$	Au2(0,0,0.325)
				$Au3(\frac{1}{2},\frac{1}{2},\frac{1}{2})$
Fe-Au (Å)	1.93	1.84	1.83	1.79
Au-Au (Å)	—	2.26	2.20	2.14
ΔE (eV)	1.439	0.732	0.522	0.335

to the value obtained for the interlayer distance in a bcc Fe crystal and Au-Fe interlayer spacing is the average of the both. Similar superstructures with tetragonal $\sqrt{a}\times\sqrt{a}\times c$ supercells are considered in Refs. 3 and 5.

The calculations start from building perfect multilayer supercells, with eight atoms in each atomic layer. The supercells have 4 or 6 monolayers and contain 32 or 48 atoms, respectively. Next, we optimize the cell sizes and the atomic positions under assumption that the symmetry of structures remains unchanged. It means that the movement of atoms is restricted to the collective displacement of all atoms belonging to one monolayer along the z direction. In Tables I and II the symbols of symmetry groups and the structural data of the optimized multilayers are presented. The in-plane lattice parameter a is consistent with the bcc Fe lattice constant. The parameter c, given by the sum of the interlayer spacings, depends on the combination of Fe and Au monolayers. The supercells used in our calculations are $2\sqrt{2}a\times 2\sqrt{2}a\times 2c$ and $2\sqrt{2}a\times 2\sqrt{2}a\times c$ for Fe_1/Au_1 and remaining structures, respectively.

The Fe_1/Au_1 monoatomic multilayer is usually consider as the tetragonal $L1_0$ ordered alloy. In our calculations, the tetragonality of Fe_1/Au_1 defined as $c/\sqrt{2}a$ is 0.975 and it is slightly larger than the experimental value of 0.94[1] and larger than the previously calculated 0.865 (Ref. 5) or 0.9.[30] In Refs. 5 and 30 the in-plane lattice constant was fixed.

As it is shown in Table I, the values of the Au-Au and Fe-Au interlayer spacing in the Fe_1/Au_n structures are larger than the values of the interlayer spacing in the bulk Au and the average value of interlayer spacings in the bulk Au and Fe, respectively. The distance between neighboring layers decreases with increasing thickness of Au spacer between Fe monolayers. In Fe_2/Au_2, Fe_2/Au_4, Fe_3/Au_3 the corresponding interlayer distances are equal or smaller than those in the Au and Fe crystals.

TABLE II. The structural properties of Fe_m/Au_n multilayers with thicker Fe layer optimized within a relevant space group. The Fe-Au, Au-Au, and Fe-Fe distances are vertical distances between neighboring layers. ΔE is the formation energy per one layer consisting of eight atoms.

Multilayer	Fe_2/Au_2	Fe_2/Au_4	Fe_3/Au_3	Fe_3/Au_1
Space group	C_{4v}^1	C_{4v}^1	D_{4h}^1	D_{4h}^1
a (Å)	3.03	2.99	2.95	2.79
c (Å)	6.59	10.75	10.27	6.79
Nonequivalent atoms	Fe1(0,0,0.334)	Fe1(0,0,0.997)	Fe1(0,0,0.128)	$Fe1(\frac{1}{2},\frac{1}{2},0.287)$
	$Fe2(\frac{1}{2},\frac{1}{2},0.216)$	$Fe2(\frac{1}{2},\frac{1}{2},0.885)$	$Fe2(\frac{1}{2},\frac{1}{2},0)$	$Fe2(0,0,\frac{1}{2})$
	Au1(0,0,0.4711)	Au1(0,0,0.725)	$Au1(0,0,\frac{1}{2})$	Au1(0,0,0)
	$Au2(\frac{1}{2},\frac{1}{2},0.779)$	$Au2(\frac{1}{2},\frac{1}{2},0.535)$	$Au2(\frac{1}{2},\frac{1}{2},0.296)$	
		Au3(0,0,0.347)		
		$Au4(\frac{1}{2},\frac{1}{2},0.156)$		
Fe-Au (Å)	1.68	1.68	1.72	1.99
Au-Au (Å)	2.03	2.04	2.09	—
Fe-Fe (Å)	1.21	1.20	1.32	1.48
ΔE (eV)	0.733	0.489	0.502	1.511

TABLE III. The calculated magnetic spin moments (μ_B) of Fe and Au atoms placed in different atomic layers of Fe_m/Au_n systems.

Layer	Fe_1/Au_1	Fe_1/Au_2	Fe_1/Au_3	Fe_1/Au_5	Fe_2/Au_2	Fe_2/Au_4	Fe_3/Au_3	Fe_3/Au_1
1	Fe 2.848	Fe 2.914	Fe 2.959	Fe 2.920	Fe 2.692	Fe 2.616	Fe 2.765	Fe 2.633
2	Au −0.014	Au 0.007	Au 0.026	Au 0.007	Fe 2.692	Fe 2.616	Fe 2.442	Fe 2.280
3		Au 0.007	Au −0.016	Au −0.019	Au 0.024	Au 0.019	Fe 2.765	Fe 2.633
4			Au 0.026	Au −0.009	Au 0.024	Au −0.008	Au 0.042	Au 0.058
5				Au −0.019		Au −0.008	Au −0.013	
6				Au 0.007		Au 0.019	Au 0.042	

In Tables I and II we also compare the formation energies per one layer of Fe_m/Au_n supercells defined as

$$\Delta E = [E_{Fe_n/Au_m} - (nE_{Fe} + mE_{Au})]/(m+n), \quad (1)$$

where E_{Fe_n/Au_m}, E_{Fe}, and E_{Au} are the total energies of multilayer supercell, Fe layer in the bulk Fe supercell, and Au layer in the bulk Au supercell, respectively. The formation of Fe_1/Au_1 and Fe_3/Au_1 costs two or three times more energy than the formation of the remaining multilayers.

In the calculations, we assume the ferromagnetic order of the iron atoms. The calculated magnetic spin moments of Fe and Au atoms within each atomic layer of Fe_m/Au_n systems are summarized in Table III. As it was shown already[4,32] the iron atoms have larger magnetic moments than in the bulk Fe. The largest values are observed for the structures with Fe monolayer. In thicker Fe multilayers, the magnetic spin moments of interface iron layers are lower than in Fe_1/Au_n. Additionally, in Fe_3/Au_3 and Fe_3/Au_1 the magnetic moments of Fe atoms placed at central Fe monolayer are considerably reduced in comparison to that placed at the interfaces. The Au layers are slightly polarized by the neighboring Fe layers.

C. Dynamical properties

Next, the phonon dispersion relations were calculated for each multilayer structure. The results are shown in Fig. 3. All studied structures with one monolayer of either Fe or Au atoms have imaginary frequencies. It means that these structures are not stable at 0 K, however, they can become stable at higher temperatures. The Fe_m/Au_n multilayers are stable when $m>1$ and $n>1$.

The direct method of the calculation of the phonon dispersion relations delivers exact phonon frequencies at special wave vectors of the Brillouin zone, which are commensurate with the supercell size, provided the supercell shape guarantees that the dynamical matrix conserves its symmetry.[23] For Fe_m/Au_n structures, the chosen supercells provide the exact frequencies at the Γ, X, Z, M, R, A, and Γ, X, M, and Γ, X, Z high-symmetry points for structures of the D^1_{4h} symmetry group (Fe_1/Au_1, Fe_1/Au_3, Fe_1/Au_5, Fe_3/Au_3, Fe_3/Au_1), $D17_{4h}$ (Fe_1/Au_2), and C^1_{4h} (Fe_2/Au_2, Fe_2/Au_4), respectively. Indeed, the unstable modes observed at X and R high-symmetry points were calculated taken into account the long-range interaction. Moreover, since the calculated force constant diminishes three orders of magnitude from the center to the surface of the supercell, all phonon branches, being a symmetry controlled interpolation between special wave vectors, are well reproduced.

In Fig. 4 the total (black line) and Fe partial (grey shaded region) phonon density of states spectra are presented. For Fe_1/Au_n (left column of Fig. 4) two sharp modes, at 4.5 and 6 THz, corresponding to the Fe atoms occur above the maximal frequency of the phonon density of states for the bulk Au. Similar effect due to different atomic masses between host and impurity atoms has been observed both experimentally and theoretically[33] for various systems with impurities. The sharp modes are not observed for multilayers with two or three neighboring Fe layers (right column of Fig. 4). For them, the frequencies of Fe atoms vibrations cover a broader frequency range and the maximal frequencies are shifted to higher values. This is in agreement with experimental studies

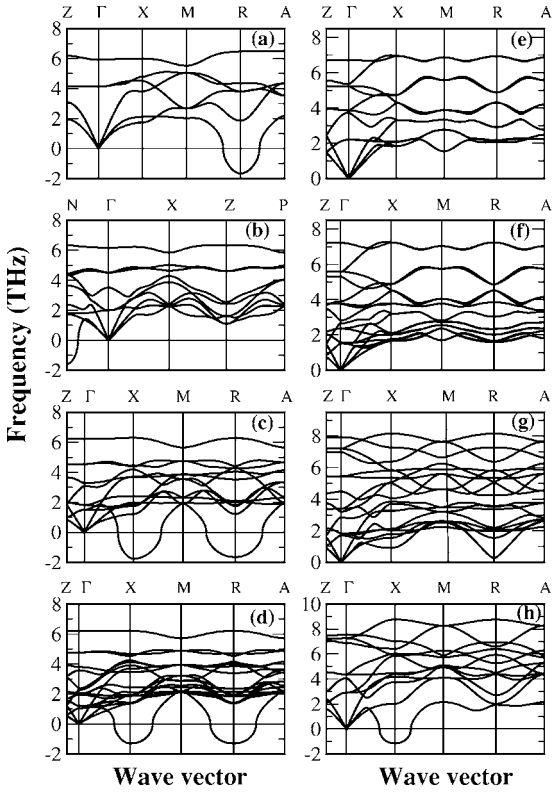

FIG. 3. The phonon dispersion relations of the different Fe_m/Au_n multilayers: (a) Fe_1/Au_1, (b) Fe_1/Au_2, (c) Fe_1/Au_3, (d) Fe_1/Au_5, (e) Fe_2/Au_2, (f) Fe_2/Au_4, (g) Fe_3/Au_3, (h) Fe_3/Au_1.

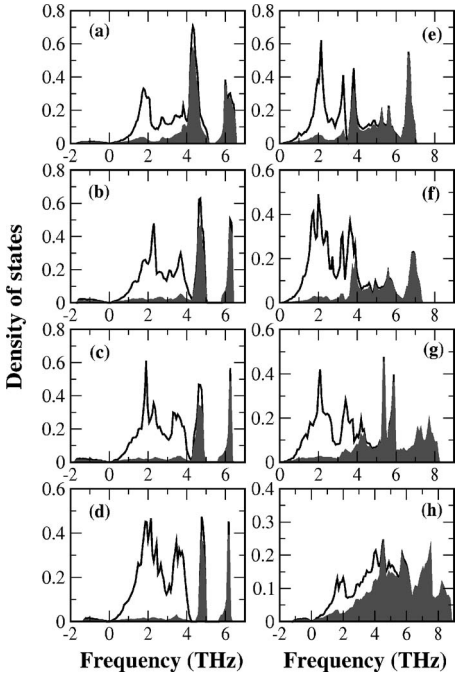

FIG. 4. The phonon density of states spectra for the different Fe_m/Au_n multilayers. The description of panels (a)–(f) corresponds to those of Fig. 2. The lines and shaded areas describe the total density of states and the Fe partial density of states, respectively.

of the phonon density of states for Fe(5 Å)/Au(5 Å), Fe(10 Å)/Au(10 Å), Fe(20 Å)/Au(20 Å) multilayers and the bcc Fe crystal.[34] The highest frequencies are observed in the bulk Fe. With decreasing thickness of Fe and Au layers, the high frequency edge is shifted towards lower frequencies.

D. The stable atomic configurations of Fe_1/Au_n multilayers

Now, we attempted to find the stable atomic configurations for multilayer structures with Fe monolayer. The atomic displacements corresponding to modes with the imaginary frequencies could generate the structures with lower ground-state energy. The polarization vector of the soft mode allows one to generate a displacement pattern corresponding to the frozen soft phonon. Such a frozen pattern is used to carry out the optimization process without the symmetry restrictions on atomic positions. The rearrangement of atoms leads to the formation of structure with lower symmetry.

1. Fe_1/Au_1

Subsequent optimization of the sizes and atomic positions of Fe_1/Au_1 structure with starting frozen soft mode pattern leads to the body-centered-tetragonal structure (space group D_{4h}^{17}) with doubled lattice constants $a=5.75$ Å and $c=7.28$ Å.[31] The reconstructed structure has no imaginary frequencies [Fig. 5(a)]. It is stable, and its ground-state energy is lower by 1920 meV per supercell than the energy of the high-symmetry structure.

Figure 6 shows atomic positions within four layers of the relaxed Fe_1/Au_1 structure (left column) together with their z components. In comparison to the high-symmetry structure, the iron atoms are shifted in (x,y) plane and the gold atoms are moved along the z direction. The nonequivalent atomic positions are Fe(0.2895,0.2895,0), Au1(0,0.5,0.25), Au2(0,0,0.1967). The symmetry operations give the positions of the remaining atoms as Fe(0.2105,0.2105,0.5) and Au(0.5,0.5,0.3033). The magnetic spin moments of iron atoms decrease from 2.85 to 2.72 μ_B. The induced magnetic spin moments of Au are positive and equal 0.017 and 0.005 for interface and interior atoms of the split layers.

Since the primitive unit cell contains eight atoms, the number of the frequency branches is now 24. The vibrations of iron atoms are localized around three frequencies [Fig. 5(c)]. The lowest at about 4.3 THz is the same as for unstable configuration [Fig. 4(a)]. Two remaining peeks at 5.8 and 6.8 THz are placed below and above the second sharp peak of the unstable Fe_1/Au_1.

2. Fe_1/Au_3

In the case of Fe_1/Au_3 two subsequent optimizations were performed. The first one was started from the displacement

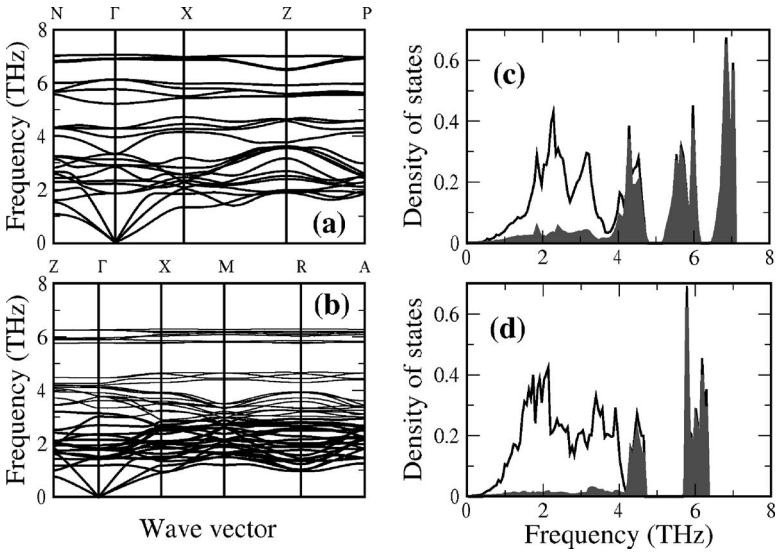

FIG. 5. The phonon dispersion relations and the phonon density of states spectra of the Fe_1/Au_1 (a) and (c) and Fe_1/Au_3 (b) and (d) stable configurations.

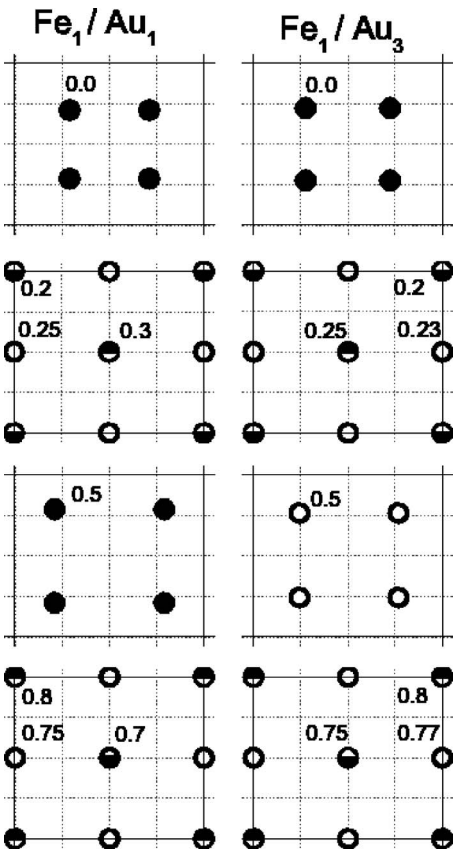

FIG. 6. The rearrangement of the atoms in each of four layers forming the Fe_1/Au_1 (left column) and Fe_1/Au_3 (right column) structures. Black circles represent Fe atoms, open and black and white circles correspond to the gold atoms. Close to the symbols the z components of atomic position are given.

pattern generated by a combination of both soft modes. It resulted in the structure with orthorhombic symmetry and lattice constants a, $2a$, and c with respect to the high-symmetry structure. Since this state also has imaginary frequencies, we repeated the optimization procedure. The resulting structure has the tetragonal symmetry, space group D_{4h}^1, the same as high-symmetry configuration, but the lattice constant, $a=5.77$ Å, is doubled. The lattice constant $c=8.04$ Å is only slightly modified. There are five nonequivalent atoms with atomic positions Fe(0.276,0.276,0), Au1(0.5,0.5,0.248), Au2(0.5,0,0.226), Au3(0,0,0.202), and Au4(0.244,0.244,0.5). In comparison to the starting structure, the iron atoms are shifted in the (x,y) plane (Fig. 6). Gold atoms of the interfacial layer are displaced in z direction, and gold atoms of the middle layer are moved in the opposite directions than corresponding atoms from iron layer. The phonon dispersion curves presented in Fig. 5(b) indicate that this structure is stable. The ground-state energy of it is lower by 540 meV per supercell than the ground-state energy of the unrelaxed structure. The difference is so subtle that it could be suppressed by the thermal motions of atoms. The magnetic spin moments of iron atoms decrease from 2.96 to 2.88 μ_B. The magnetic spin moments of Au atoms located within the first split layer are 0.019, 0.030, 0.032 for $z=0.202$, 0.226, 0.248, respectively. The values of magnetic moments of the middle Au layer remain almost unchanged, -0.017 μ_B.

IV. CONCLUSIONS

We have calculated the phonon dispersion relations for perfectly ordered Fe_m/Au_n multilayers. The multilayers with Fe and Au layer thickness of two or more monolayers have the only positive vibrational frequencies, thus they can form a stable structures without any rearrangement of atoms. The imaginary frequencies obtained for Fe_m/Au_n with Fe or Au monolayer show that these structures are unstable. The stable configuration can be formed after the condensation of the soft phonon mode. Thus, using the displacement pattern of soft modes, the stable lower-symmetry configurations for Fe_1/Au_1 and Fe_1/Au_3 were found. In comparison to the high-symmetry structures, the Fe atoms are shifted from their initial positions in (x,y) plane only. The displacements of 0.32 Å and 0.17 Å for Fe_1/Au_1 and Fe_1/Au_3, respectively, are observed. The reconstruction is accompanied by doubly larger lattice constants of Fe_1/Au_1 and by doubling the in-plane lattice constant of Fe_1/Au_3. The gain of the total energy of the high-symmetry structure in comparison to the reconstructed structures are 60 and 17 meV/atom for Au monolayer and Au trilayer structures, respectively.

Electron band structure calculations predict enhanced magnetic moments in the magnetic-nonmagnetic multilayers due to the reduction of the number of the next-neighboring atoms. In accordance to Refs. 4 and 32, the enhanced Fe magnetic moments and the small induced magnetic moments of Au are observed in all studied multilayers. In Fe_1/Au_1 and Fe_1/Au_3, the magnetic moments of iron atoms slightly decrease after the rearrangement of atoms towards the stable configuration.

Although, the formation of good quality Fe_m/Au_n multilayers with the atomic layer thickness larger than one monolayer, by the so-called atomic layer deposition, is evidenced by different experimental technique, the obtained Fe_1/Au_1 structures always have limited degree of order. The ordering process in which monoatomic layers of Au and Fe are stacked alternately forming the AuFe ordered alloy of $L1_0$ structure seems to be influenced by the complicated growth of Fe monolayer on the Au surface, as shown by the atomic scale scanning tunneling microscopy investigation.[35,36] The CEMS measurements for this system verified the existence of the $L1_0$ phase.[3,18] The authors conclude that the amount of the $L1_0$ phase is only 30% of that expected for the perfect growth and the resulting structure may be regarded as a mixture of Fe_1/Au_1 and Fe_2/Au_2 structures. Now, in terms of our results, the complex CEMS spectra for Fe_1/Au_1 can be interpreted as generated by the meaningful electric field gradient acting on Fe atoms displaced from its high-symmetry positions.

Since the calculated mismatch is larger than experimental one the stabilization of the relaxed Fe_1/Au_1 and Fe_1/Au_3 structures could be caused by misfit stresses introduced to these artificial systems. The calculated misfit of the bulk in-

plane interatomic distance is 2.4%, while the experimental one is only 0.6%. Since the multilayers in question form a common electronic band structure, it is not possible at the moment to judge whether the reconstructed phases are the direct consequence of the mentioned misfit. Additional studies are needed to resolve this question.

ACKNOWLEDGMENTS

The work was partially supported by the European Community under FP6 Contract No. NMP4-CT-2003-001516 (DYNASYNC). The authors thank P. T. Jochym, J. Łażewski, and P. Piekarz for valuable discussion.

[1] K. Takanashi, S. Mitani, M. Sano, H. Fujimori, H. Nakajima, and A. Osawa, Appl. Phys. Lett. **67**, 1016 (1995).
[2] S. Mitani, K. Takanashi, H. Nakajima, K. Sato, R. Schreiber, P. Grünberg, and H. Fujimori, J. Magn. Magn. Mater. **156**, 7 (1996).
[3] L. Uba, S. Uba, V. N. Antonov, A. N. Yaresko, T. Ślęzak, and J. Korecki, Phys. Rev. B **62**, 13731 (2000).
[4] J.-T. Wang, Z.-Q. Li, Q. Sun, and Y. Kawazoe, J. Magn. Magn. Mater. **183**, 42 (1998).
[5] Z. P. Shi, J. F. Cooke, Z. Zhang, and B. M. Klein, Phys. Rev. B **54**, 3030 (1996).
[6] L. Szunyogh, B. Ujfalussy, P. Weinberger, and C. Sommers, Phys. Rev. B **54**, 6430 (1996).
[7] J. Unguris, R. J. Celotta, and D. T. Pierce, Phys. Rev. Lett. **79**, 2734 (1997).
[8] J.-T. Wang, L. Zhou, D.-S. Wang, and Y. Kawazoe, Phys. Rev. B **62**, 3354 (2000).
[9] A. Yoshihara, J.-T. Wang, K. Takanashi, K. Himi, Y. Kawazoe, H. Fujimori, and P. Grünberg, Phys. Rev. B **63**, 100405(R) (2001).
[10] J. Opitz, P. Zahn, J. Binder, and I. Mertig, Phys. Rev. B **63**, 094418 (2001).
[11] D. T. Dekadjevi, P. A. Ryan, B. J. Hickey, B. D. Fulthorpe, and B. K. Tanner, Phys. Rev. Lett. **86**, 5787 (2001).
[12] T. Mizuno, Y. Aoki, H. Sugawara, H. Sato, K. Takanashi, S. Mitani, and H. Fujimori, J. Magn. Magn. Mater. **240**, 358 (2002).
[13] T. L. Monchesky, A. Enders, R. Urban, K. Myrtle, B. Heinrich, X.-G. Zhang, W. H. Butler, and J. Kirschner, Phys. Rev. B **71**, 214440 (2005).
[14] K. Takanashi, S. Mitani, K. Himi, and H. Fujimori, Appl. Phys. Lett. **72**, 737 (1998).
[15] K. Takanashi, S. Mitani, H. Fujimori, K. Sato, and Y. Suzuki, J. Magn. Magn. Mater. **177-181**, 1199 (1998).
[16] K. Sato, E. Takeda, M. Akita, M. Yamagutchi, K. Takanashi, S. Mitani, H. Fujimori, and Y. Suzuki, J. Appl. Phys. **86**, 4985 (1999).
[17] T. Ślęzak, W. Karaś, M. Kubik, M. Mohsen, M. Przybylski, N. Spiridis, and J. Korecki, Hyperfine Interact. **C3**, 409 (1998).
[18] J. Korecki, M. Kubik, N. Spiridis, and T. Ślęzak, Acta Phys. Pol. A **97**, 129 (2000).
[19] W. Karaś, B. Handke, K. Krop, M. Kubik, T. Ślęzak, N. Spiridis, D. Wilgocka-Ślęzak, and J. Korecki, Phys. Status Solidi A **189**, 287 (2002).
[20] G. Kresse and J. Hafner, Phys. Rev. B **47**, 558 (1993); **49**, 14251 (1994).
[21] G. Kresse and J. Furthmüller, Software VASP, Vienna, 1999; Phys. Rev. B **54**, 11169 (1996); Comput. Mater. Sci. **6**, 15 (1996).
[22] P. E. Blöchl, Phys. Rev. B **50**, 17953 (1994); G. Kresse and D. Joubert, *ibid.* **59**, 1758 (1999).
[23] K. Parlinski, Z. Q. Li, and Y. Kawazoe, Phys. Rev. Lett. **78**, 4063 (1997).
[24] K. Parlinski, Software PHONON, Cracow, 2003.
[25] A. Dal Corso and S. de Gironcoli, Phys. Rev. B **62**, 273 (2000).
[26] *Magnetic Properties of Metals d-Elements, Alloys and Compounds*, Data in Science and Technology, edited by H. P. J. Wijn (Springer, Berlin, 1991).
[27] E. G. Moroni, G. Kresse, J. Hafner, and J. Furthmüller, Phys. Rev. B **56**, 15629 (1997).
[28] J. W. Lynn, H. G. Smith, and R. M. Nicklow, Phys. Rev. B **8**, 3493 (1973).
[29] B. N. Brockhouse, H. E. Ahou-Helal, and E. D. Hallman, Solid State Commun. **5**, 211 (1967); M. W. Finnis, K. L. Kear, and D. G. Pettifor, Phys. Rev. Lett. **52**, 291 (1984).
[30] J.-T. Wang, Z.-Q. Li, and Y. Kawazoe, J. Phys.: Condens. Matter **9**, 4549 (1997).
[31] H. T. Stokes and D. M. Hatch, ISOTROPY, 2002, stokes.byu.edu/isotropy.html
[32] M. Böhm and U. Krey, J. Magn. Magn. Mater. **192**, 27 (1999).
[33] K. Parlinski, P. T. Jochym, O. Leupold, A. I. Chumakov, R. Rüffer, H. Schober, A. Jianu, J. Dutkiewicz, and W. Maziarz, Phys. Rev. B **70**, 224304 (2004).
[34] E. E. Alp, W. Sturhahn, and T. S. Toellner, Hyperfine Interact. **153**, 295 (2001).
[35] V. Blum, Ch. Rath, S. Muller, L. Hammer, K. Heinz, J. M. Garcia, and J. E. Ortega, Phys. Rev. B **59**, 15966 (1999).
[36] N. Spiridis and J. Korecki, Appl. Surf. Sci. **141**, 441 (2000).